터널과 지하공간, 한국암반공학회지
Vol. 13, No. 3, 2003, pp. 180~186

TUNNEL & UNDERGROUND SPACE, Vol. 13, No. 3, 2003, pp. 180-186
Journal of Korean Society for Rock Mechanics

Influence of Rock Inhomogeneity on the Dynamic Tensile Strength of Rock

Sang Ho Cho[1], Hyung Sik Yang[2] and Katsuhiko Kaneko[1]

암석의 동적 인장강도에 미치는 불균질성의 영향

조상호, 양형식, Katsuhiko Kaneko

Abstract. The fracture processes under dynamic loading in tension were simulated using a proposed numerical approach and analyzed to determine dynamic tensile strength. The dynamic tensile strength and the scatter of the strength data decreased with increasing uniformity coefficients. The differences of static and dynamic tensile strength were due to the stress concentrations and redistribution mechanisms in the rock specimen. Although there were different mechanisms for the static and dynamic fracture processes, the static and dynamic tensile strengths were close to the mean microscopic tensile strength at high values of the uniformity coefficient. This paper shows that the rock inhomogeneity has an effect on dynamic tensile strength and is a factor that contributes to the different specimen strengths under dynamic and static loading conditions.

KeyWords: Fracture processes, Dynamic tensile strength, Uniformity coefficients, Microscopic tensile strength, Rock inhomogeneity

초 록. 동적 인장강도를 평가하기 위해 수치해석기법을 이용하여 흡킨슨효과를 가정한 동적 인장시험의 암석 파쇄 과정을 해석하였다. 동적 인장 파쇄 과정과 정적 인장 파쇄 과정에 명확한 차이가 있음을 밝혔으며, 동적 인장강도와 정적 인장강도의 상위는 응력집중현상과 응력재분배에 의해 발생된다는 것을 지적하였다. 그러나 정적파쇄와 동적파쇄 과정에 큰 차이가 있음에도 불구하고 정적 인장강도와 동적 인장강도는 미시적 인장강도의 균질성 계수가 증가함에 따라 미시적 인장강도의 평균치에 근접하였다. 본 연구로부터 암석의 불균질성은 동적 인장강도에 영향을 미치는 요인이며, 동적 인장강도와 정적 인장강도의 상위를 발생시키는 중요한 요인임을 지적하였다.

핵심어: 파쇄 과정, 동적 인장강도, 균질성 계수, 미시적 인장강도, 암석 불균질성

1. Introduction

The dynamic tensile strength of rock is important in breaking of rock by explosives. The dynamic tensile strength can exceed the static tensile strength by as much as one order of magnitude (Bacon 1962, Rinehart 1965 and Ma et al., 1998). Hino (1956) proposed the fundamental principal of rock failure in blasting using shock wave theory, and developed a method to determine the dynamic tensile strength of rock materials from the velocities of the rock fragments created by the detonation of an explosive charge. He used a high-speed camera and a chronotron millisecond meter to measure the fragment velocities. He reported that the dynamic tensile strength of rock estimated from the velocity measurements was more than double the static tensile strength.

In the accompanying paper (Part I, Cho et al. 2003), the influence of inhomogeneity of rock on static tensile strength was revealed by means of the numerical approach, based on finite element method and fracture mechanics. In this study, the numerical approach was modified to simulate fracture processes of rock specimens under dynamic loading conditions.

[1]Graduate School of Eng., Hokkaido Univ., Sapporo, Japan
[2]Dep. Geosystem Eng., Chonnam Nat'l Univ., Korea
접수일: 2003년 3월 6일
심사 완료일: 2003년 4월 18일

The dynamic tensile strengths were estimated from the fracture process to verify an influence of inhomogeneity of rock on the dynamic tensile strengths and compared with the static tensile strength estimated in the accompanying paper.

2. Numerical Simulation Approach

Rock is an inhomogeneous material, and the inhomogeneity plays a significant role in the fracture process. The strength and elastic modulus may be used to model the rock inhomogeneity. In this study, Weibull's distribution (1951), which considers the microscopic strength of rocks, was employed. Consider the microscopic strength x_t in a volume V. The cumulative probability distribution $G(V,x_t)$ is

$$G(V,x_t)=1-exp\left[-\frac{V}{V_0}\left(\frac{x_t}{\bar{x}_t(V_0)}\right)^m\Gamma^m\left(1+\frac{1}{m}\right)\right] \quad (1)$$

where Γ is the Gamma function, m is the coefficient of uniformity, V_0 is the reference volume, and $\bar{x}_t$ is the mean microscopic strength. Random numbers satisfying Weibull's distribution were generated to give the spatial distribution of the microscopic strengths in the analysis model. To simulate the fracture process under dynamic loading, the increment displacement form (1995) of a dynamic finite element method was used, based on the Newmark-β method (1959). The equation of motion with respect to time t is

$$M\ddot{u}(t)+C\dot{u}(t)+Ku(t)=f(t) \quad (2)$$

where the vector f is the sum of the externally applied loads, the vectors $\ddot{u}$, $\dot{u}$ and u denote the acceleration, velocity, and displacement of all of the nodes, and M, C, and K denote the mass, viscous, and stiffness matrices. The detailed explanations for the numerical simulation approach used in this study have been introduced in the reference (Cho et al. 2003).

3. Fracture Process Simulation in Dynamic Loading Condition

The analysis model consisted of one loading boundary and three free boundaries, as shown in Fig. 1. The model was 0.2 m in length and 0.02 m in height and had a peak pressure of 20 MPa, a rise time of 1 μs, and a decay time of 50 μs. The models were divided into triangular elements consisting of 4221 nodal points. The parameters and calculation conditions are listed in Table 1. Random numbers satisfying Weibull's distribution were generated to give the spatial distribution of the microscopic strengths. Figure 2

Table 1. Mechanical properties and calculation conditions for the analysis model.

Parameter	Value
Density ρ (kg/m^3)	2500
Elastic modulus E (GPa)	40
Poisson's ratio ν	0.25
Average compressive strength S_c (MPa)	60
Average tensile strength S_t (MPa)	4.0
Fracture energy G_f (Pa · m)	0
Coefficient of uniformity m	5,50 and ∞
Time step Δt(μs)	0.02
P wave velocity C_P (m/s)	4381
S wave velocity C_s (m/s)	2529
Bar velocity C_b (m/s)	4000

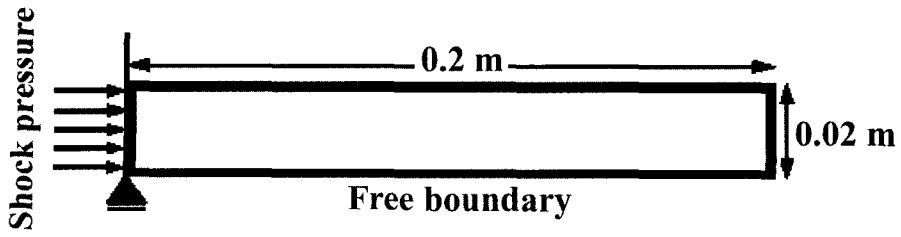

Fig. 1. Geometry of the model subjected to dynamic loading.

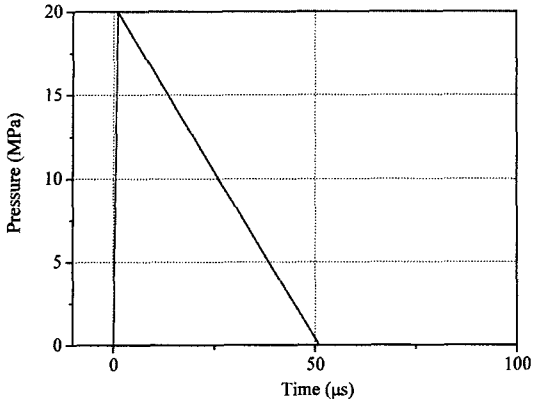

Fig. 2. Pressure-time curves.

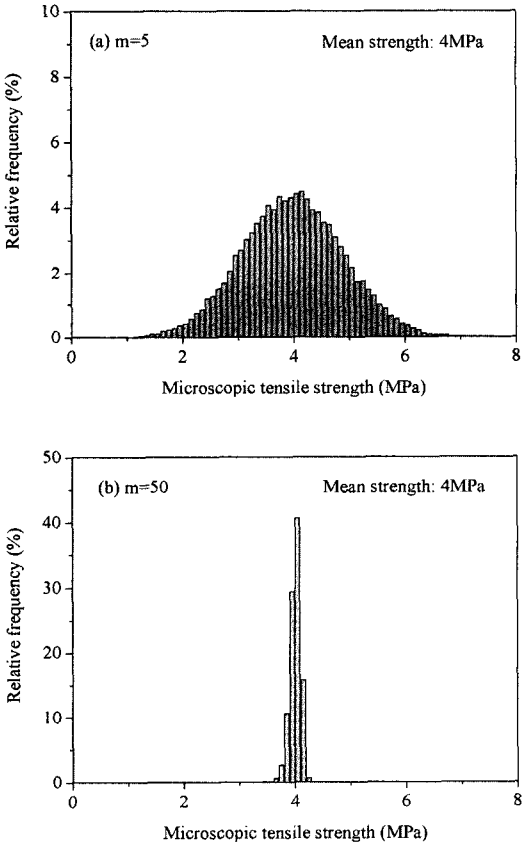

Fig. 3. Distribution of the microscopic tensile strength in the analysis model when (a) m=5 and (b) m=50.

shows the microscopic tensile strength distributions when m=5 and m=50. Here, the mean tensile strength is 4 MPa, m=5 corresponds to inhomogeneous materials, and m=50 corresponds to comparatively homogeneous

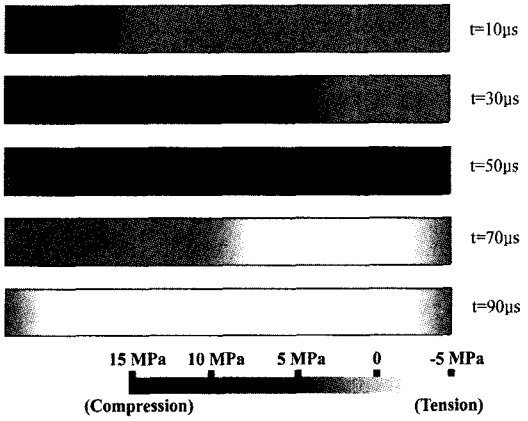

Fig. 4. Axial stress distribution in the specimen without fractures.

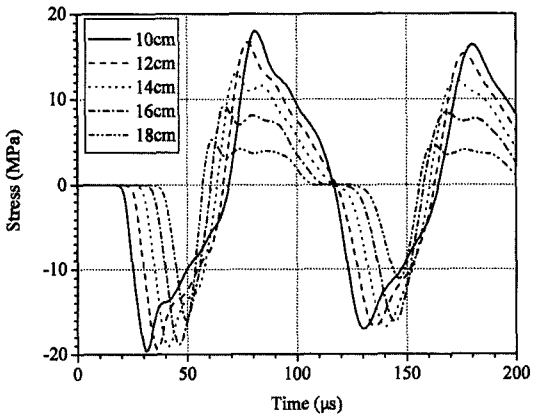

Fig. 5. Axial stress-time curves in the specimen without fractures.

materials. Figure 3 shows the pressure-time curve for the analysis models. The curve was loaded as incident pressure at the loading boundary. First of all, to evaluate the tensile stress in a specimen subjected to an input pressure, a specimen that did not fracture was simulated. Figure 4 shows the axial stress distributions. Here, the axial indicates horizontal direction, black color shows compressive stress and white color represents tensile stress. An incident compressive stress wave is propagated and reflected as a tensile wave at the free end, and the tail of the incident compressive wave are superposed and this superposed wave develops the tensile stress as shown at 70 μs. Figure 5 shows the stress-time curves with a distance from the boundary. The stress curves near the free

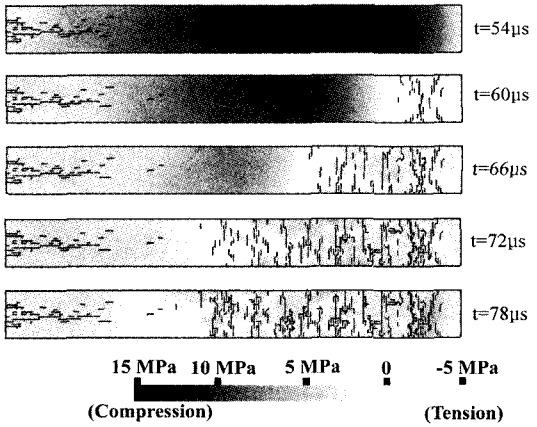

Fig. 6. Distribution of the axial stress and crack propagation process in a specimen when m=5.

end caused by the reflected tensile waves were rapidly changed into tension.

The fracture processes were simulated using specimens with ten different microscopic strength spatial distributions when m=5 and m=50. The axial stress distribution and crack propagations in a specimen with different microscopic strength spatial distributions when m=5 are given in Fig. 6. The compressive stress wave caused by the incident pressure reached the free end of the specimen at 54 μs and was reflected as a tension wave. The tensile wave was superimposed upon the tail of the compressive stress wave, and developed an increasing amount of tension. It started to produce a large number of microcracks at 60 μs.

Figure 7 (a) shows the crack patterns in specimens with different microscopic strength spatial distributions when m=5. The first fractures that were formed and have comparatively large crack open displacement were selected as the fracture planes, as indicated by the triangles. The positions of the fracture plane varied with the microscopic strength spatial distribution. While the positions of the fracture plane didn't vary significantly when m=50 as shown in Fig. 7 (b).

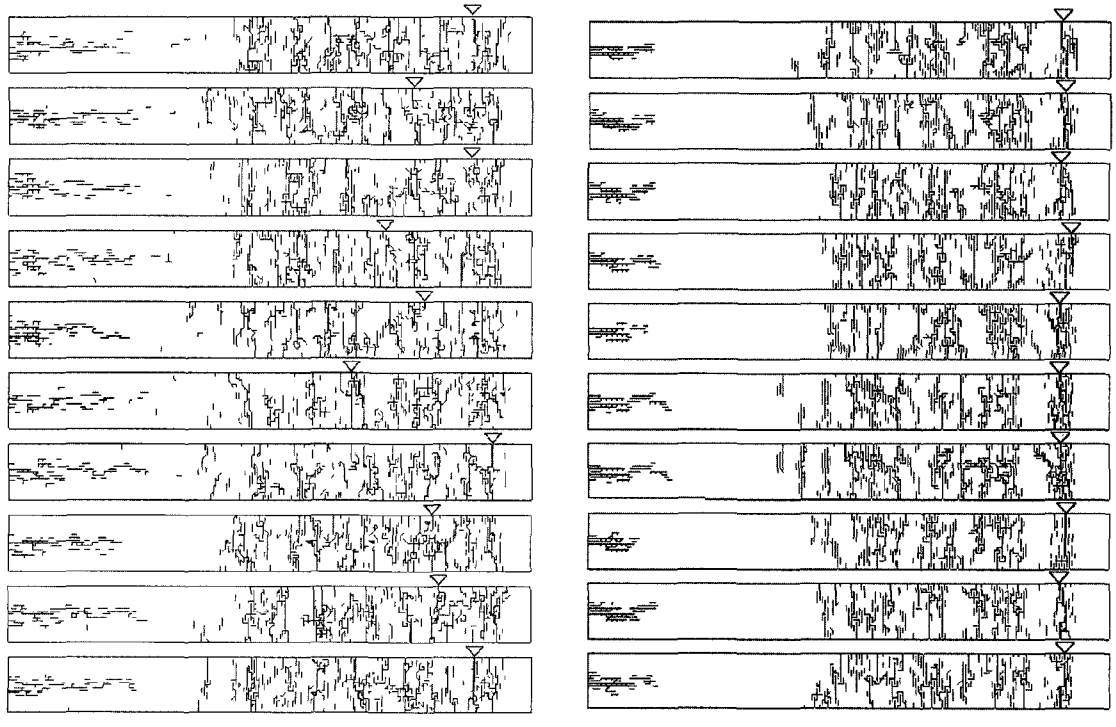

Fig. 7. Fracture and crack patterns with various spatial microscopic strength distributions when (a) m=5 and (b) m=50. The triangular symbols indicate the fractures.

4. Determination of the Dynamic Tensile Strength

When an incident compressive stress wave in a material is reflected as a tensile wave at the free end, the reflected wave and the tail of the incident compressive wave are superposed. The superposed wave develops into a tensile stress wave, which generates fractures near the free end of the material. The tensile stress at the fracture is the dynamic tensile strength of the material. From this point of view, we tried to determine dynamic tensile strength from maximum tensile stress experienced in the specimen that did not fracture. Figure 8 shows maximum tensile stress in the specimen without fractures. Tensile stress in a specimen corresponds to the fracture position of a specimen was adapted as the tensile stress of the specimen.

The determined dynamic tensile strengths when m=5, 50, and ∞ are listed in Table 2. The dynamic tensile strengths varied from 5.231 to 11.99 MPa when m=5, and from 5.147 to 5.394 MPa when m=50. The dynamic tensile strengths when m= ∞ were almost the same as the mean microscopic tensile strength, although there were some slight differences. The mean dynamic tensile strength decreased with increasing m. The stress rates $\dot{\sigma}$ could be derived from the stress wave time curve in a specimen without fractures at the position that corresponded to the fracture plane in a fractured specimen. The strain rates were determined from the stress rate and elastic modulus E. The strain rates varied from 4.1 to 11.4 s^{-1} when m=5, and from 4.3 to 9.6 s^{-1} when m=50. These mean that although a specimen is subjected to the same dynamic tensile loading, the specimen may show the strain rate dependency of the dynamic tensile strength due to the rock inhomogeneity.

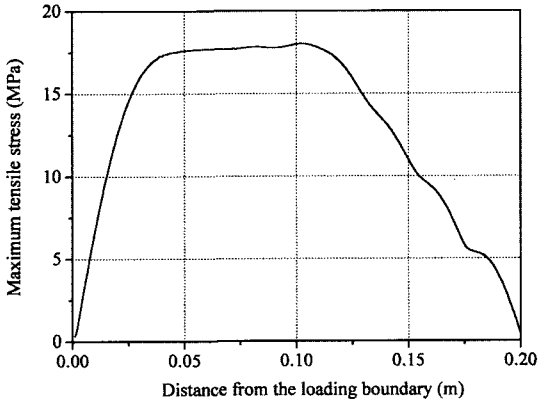

Fig. 8. Maximum tensile stress experienced in the specimen without fractures.

5. Influence of Rock Inhomogeneity and Discussion

Figure 9 (a) and (b) show the distribution of dynamic tensile strengths m=5 and 50. The range of dynamic tensile strengths became small at high uniformity coefficients. The dynamic tensile strength and the scatter of the strength data decreased with increasing uniformity coefficients. These support that rock inhomogeneity has an effect on dynamic tensile

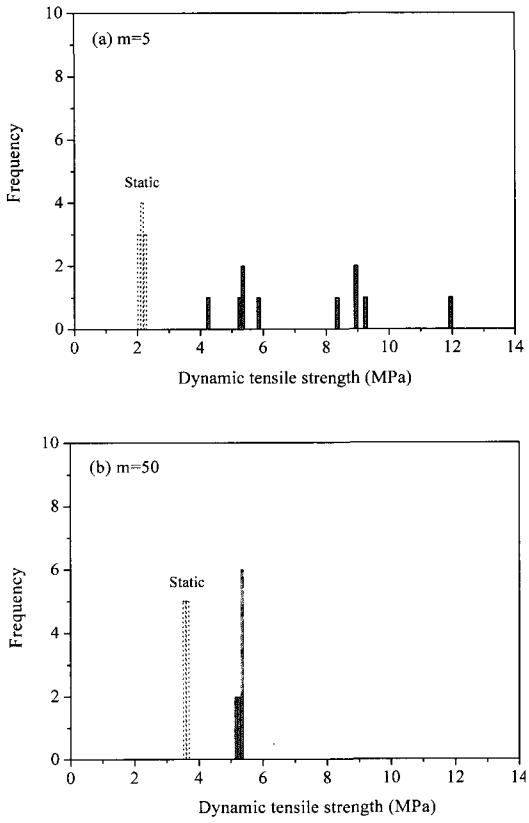

Fig. 9. Distribution of the dynamic tensile strengths when (a) m=5 and (b) m=50.

strength.

In the specimens under dynamic loading, the tensile stress field developed microcracks near the free end, as shown at 60 μs in Fig. 6. Contrary to the static situation the stress redistribution was completed throughout the entire specimen, as described in the accompanying paper (Part I, Cho et al. 2003), the stress redistribution field was localized in the region that was subjected to the reflected stress wave. The element that had the lowest microscopic tensile strength did not necessarily have an opportunity to participate in the fracture process. This can lead to strengths that are higher than the static tensile strength, because the dynamic tensile strength is generally determined from the tensile stress at the fracture, which increases with time. It is worthy noting that the differences of static and dynamic tensile strength were due to the stress concentrations and redistribution mechanisms in the rock specimen.

To compare the dynamic and static tensile strengths, the static tensile strengths represented in the accompanying paper (Part I, Cho et al. 2003) were displayed Figs. 9 (a) and (b). Although there are different mechanisms for the static and dynamic fracture processes, the static and dynamic tensile strengths were close to the mean microscopic strength at high values of the uniformity coefficient. Therefore, the inhomogeneity of the rock is a factor that contributes to the different specimen strengths under dynamic and static loading conditions.

Even in the homogenous models, $m=\infty$, the dynamic tensile strengths were slightly different from the mean microscopic tensile strength, as shown in Table 2. Moreover, the difference increased at higher strain rates. The difference is possibly due to variations in the position of the fracture plane due to stress variations, caused by specimen surface waves that correspond to Lamb's wave (1904). The variations of stress at the tail of the incident compressive stress in Fig. 4 and the oscillations that follow the peak values at 18 cm in Fig. 5 also suggest the presence of surface waves. These imply that the dynamic tensile strengths obtained using the experimental approach, based on Hopkinson's effect, could be also influenced by a surface wave.

Table 2. Dynamic tensile strength.

	Dynamic tensile strength S_d (MPa)		
	m=5	m=50	m=∞
1	5.305	5.305	4.9
2	5.821	5.231	
3	5.352	5.353	
4	8.964	5.147	
5	8.367	5.394	
6	11.99	5.352	
7	4.289	5.351	
8	8.964	5.232	
9	9.266	5.305	
10	5.231	5.147	
Mean value	7.35±2.363	5.28±0.088	4.9

6. Conclusion

The fracture processes under dynamic loading conditions were analyzed with a proposed numerical approach to determine dynamic tensile strength. The determined dynamic tensile strengths varied from 5.231 to 11.99 MPa when m=5, and from 5.147 to 5.394 MPa when m=50. The dynamic tensile strengths when m= ∞ were almost the same as the mean microscopic tensile strength. The dynamic tensile strength and the scatter of the strength data decreased with increasing uniformity coefficients. Therefore, it could be concluded that rock inhomogeneity has an effect on dynamic tensile strength. It was discussed that the differences of static and dynamic tensile strength were due to the stress concentrations and redistribution mechanisms in the rock specimen and the inhomogeneity of the rock was a factor that contributes to the different specimen strengths under dynamic and static loading conditions.

Acknowledgement

The authors wish to thank their research assistants, Mr. Kato Massaji for his helpful discussion and Ms. Nohara Sayaka for her computational assistance.

References

1. Bacon, L. 1962, A method of determining dynamic

tensile strength of rock at minimum loading. USBMRI 6067, 22.
2. Cho, S.H., Hyung Sik Yang and Kaneko, K., Influence of rock inhomogeneity on the static tensile strength of rock. J. of Korean Society for Rock Mech.(submitted)
3. Hino, K. Velocity of rock fragmentation and shape of shock wave. J. Industrial Explosives Society, 1956; 17(4): 236-241.
4. Kaneko, K., Matsunaga, Y., and Yamamoto, M. Fracture mechanics analysis of fragmentation process in rock blasting. J. Jpn Explosive Society, 1995; 58(3): 91-99 [in Japanese].
5. Lamb, H. On the propagation of tremors over the surface of an elastic solid. Phil. Trans., 1904; A: 203.
6. Ma, G., Miyake, A., Ogawa, T., Wada, Y., Ogata, Y., Seto, M., and Katsuyama, K. Study on the tensile strength of brittle materials under high stress rate using the technique based on Hopkinson's effect. J. Jpn Exp. Soc., 1998; 59(2): 49-56 [in Japanese].
7. Newmark, N.M. A method of computation for structure dynamics. Proc. ASME EM-3. 1959; 67-94.
8. Rinehardt, J.S. Dynamic fracture strength of rocks. Proc. 7th Symp. Rock Mech., Univ. Park, Penn., 1965; 205-208.
9. Weibull, W. A statistical distribution function of wide applicability. J. Appl. Mech., 1951; 18: 293-297.

조 상 호

1998년 전북대학교 자원공학과, 공학사
2000년 전남대학교 자원공학과, 공학석사

Tel: +81-11-706-6325
E-mail: chosh@geo-er.eng.hokudai.ac.jp
현재 북해도대학 대학원공학연구과 박사과정

Katsuhiko Kaneko

1970년 교토대학 자원공학과 공학사
1972년 교토대학 대학원공학연구과 공학석사
1986년 교토대학 대학원공학연구과 공학박사

Tel: +81-11-706-6322
E-mail: kaneko@geo-er.eng.hokudai.ac.jp
현재 북해도대학 대학원공학연구과 교수

양 형 식

1979년 서울대학교 자원공학과 공학사
1981년 서울대학교 대학원 자원공학과 공학석사
1987년 서울대학교 대학원 자원공학과 공학박사
Tel: 062-530-1724
E-mail: hsyang@chonnam.ac.kr
현재 전남대학교 건설지구환경공학부 교수